The Astrophysical Journal Letters, 718:L176–L180, 2010 August 1 doi:10.1088/2041-8205/718/2/L176

DIRECT EVIDENCE FOR GRAVITATIONAL INSTABILITY AND MOONLET FORMATION IN SATURN's RINGS

K. Beurle, C. D. Murray, G. A. Williams, M. W. Evans[1], N. J. Cooper, and C. B. Agnor
Astronomy Unit, Queen Mary University of London, Mile End Road, London E1 4NS, UK; C.D.Murray@qmul.ac.uk
Received 2010 March 3; accepted 2010 June 30; published 2010 July 14

ABSTRACT

New images from the *Cassini* spacecraft reveal optically thick clumps, capable of casting shadows, and associated structures in regions of Saturn's F ring that have recently experienced close passage by the adjacent moon Prometheus. Using these images and modeling, we show that Prometheus' perturbations create regions of enhanced density and low relative velocity that are susceptible to gravitational instability and the formation of distended, yet long-lived, gravitationally coherent clumps. Subsequent collisional damping of these low-density clumps may facilitate their collapse into ∼10–20 km contiguous moonlets. The observed behavior of the F ring is analogous to the case of a marginally stable gas disk being driven to instability and collapse via perturbations from an embedded gas giant planet.

Key words: instabilities – planets and satellites: dynamical evolution and stability – planets and satellites: formation – planets and satellites: rings – planet–disk interactions

1. INTRODUCTION

Saturn's ring system is the only local example of an astrophysical disk in which the competing effects of collisions and self-gravity can be studied in situ by spacecraft (Porco et al. 2005). In the main rings, the near-circular orbits of the ring particles ensure that internal collisions are less disruptive because the relative velocities are small (∼mm s^{-1}). However, self-gravity is important and is believed to be responsible for the wake structures in the A ring indirectly detected using *Cassini* data (Colwell et al. 2006; Hedman et al. 2007; Porco et al. 2008). In addition, unusual structures at the edge of the A ring and the Encke gap have been attributed to enhanced kinematical and self-gravitational effects associated with the squeezing of streamlines (Porco et al. 2005; Lewis & Stewart 2005). What has often been assumed, but never verified by observation, is the process of accretion in a planetary ring.

2. THE F RING REGION

Located between the orbits of its two shepherding satellites, Prometheus and Pandora, the F ring lies 3500 km beyond the edge of Saturn's main ring system. Initial observations from the *Cassini* spacecraft (Porco et al. 2005) revealed a multi-stranded ring with a bright core and periodic azimuthal structure associated with perturbations from the inner shepherding satellite, Prometheus. Every 14.7 hr the satellite reaches its apoapse and imposes a characteristic "streamer-channel" pattern on the ring, its "strands", and surrounding material. The subsequent Keplerian shearing of this perturbed material downstream from the encounter can easily be detected in images of the ring, and every 67.6 days the same region experiences another Prometheus encounter (Murray et al. 2005, 2008); more distant and less massive Pandora produces its own, less obvious pattern.

Several lines of evidence suggest the existence of additional objects in the F ring system: (1) the strands are now known to be spiral in nature and the result of sheared jets of debris from collisions between several small (radius ∼5–10 km) objects orbiting in the region and the core of the F ring (Murray et al. 2008; Charnoz et al. 2005; Charnoz 2009); (2) additional analysis of high-resolution *Cassini* images of the F ring (Figure 3 of Murray et al. 2008) has revealed the presence of "fans" (sequences of sheared channels with a common point of intersection covering ∼0.°5 in longitude) indicative of the perturbing effect of embedded masses (radii ∼5 km assuming a density comparable to that of Prometheus) on orbits close to that of the F ring core but with eccentricities differing from it by $\sim 10^{-4}$ (Williams 2009)[2]; and (3) numerous ($\sim 10^2$) bright features in the F ring have been attributed to the existence of ∼1 km diameter objects associated with the F ring core (Murray et al. 2008). At least some of these objects are likely related to occultation features detected close to the F ring (Esposito et al. 2008).

Many of these lines of evidence can be seen in Figure 1 which shows the same 40° section of the F ring captured in five successive sets of observations between 2007 February 27 and 2007 May 5; the radial extent of each reprojected mosaic is 400 km. A shearing jet is seen above the core in Figures 1(b)–(d) and two fans have been detected in the images. Numerous features are detectable in the core and their spacing of ∼3° is consistent with Prometheus perturbations. Furthermore, many of these features can be seen moving in either direction with respect to the core. These drifts correspond to a typical displacement from the semimajor axis of the core of ∼5 km. In Figure 1(a) Prometheus has a corotating longitude of 168°, ∼33° to the right of the displayed segment. During successive sequences, it traverses the F ring before encountering the displayed ring segment again between 2007 April 18 and May 5 (the dates of Figures 1(d) and (e)). Note that most of the features in the core survived another passage of Prometheus, although clearly the core in Figure 1(e) appears as disrupted and distorted as that in Figure 1(a), which has also just experienced passage by Prometheus. Therefore there is good evidence that Prometheus produces features in the F ring's core and that these bright objects are long-lived, perhaps surviving multiple passages of the satellite.

[1] Current address: Department of Astronomy, Cornell University, Ithaca, NY 14853, USA.

[2] Note that "fans" and "wakes" (see, e.g., Showalter et al. 1986) are both indicative of nearby, perturbing objects. The mechanism is essentially the same but the key difference is that the objects producing "fans" are on relatively eccentric orbits (Williams 2009).

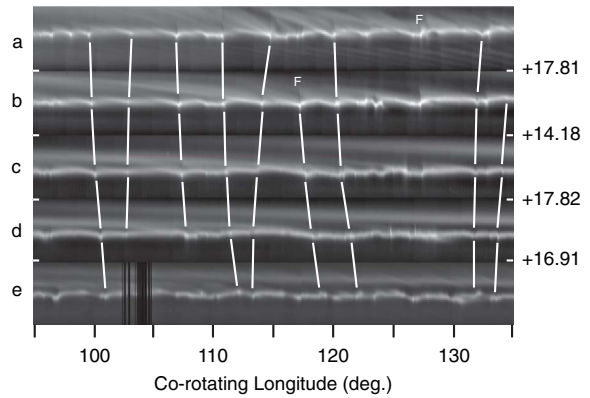

Figure 1. Sections of five, successive, reprojected mosaics of the F ring covering 40° in longitude and 400 km in radial width, displayed in a corotating frame using the mean motion of the F ring at an epoch of 12:00 UTC on 2007 January 1. The images were obtained on 2007 (a) February 27, (b) March 17, (c) March 31, (d) April 18, and (e) May 5. The time interval in days between the mid-times of the successive mosaics is shown at the right. The letter F denotes the location of a fan in the full resolution image. The lines connecting the clumps indicate a sample of possible identifications of the same object.

The existence of a moonlet belt at this location was originally proposed to explain the charged particle environment measured by Pioneer 11 (Cuzzi & Burns 1988). Although such a system could result from a collision between larger objects, its location at 2.32 Saturn radii means that the F ring is in the Roche zone (Murray & Dermott 1999) where accretion processes due to self-gravity continually compete with disruption due to collisions and tidal forces (Barbara & Esposito 2002; Canup & Esposito 1995). While it is tempting to consider some or all of the numerous objects in the F ring region as accretion products, until now there has been no direct observational evidence of such a process in any planetary ring.

3. OBSERVATIONS OF "FAN" STRUCTURES

Figure 2 shows three separate mosaics of 28° sections of the F ring constructed from reprojected *Cassini* Imaging Science Subsystem (Porco et al. 2004) images taken on three occasions between 2008 July and 2009 April. The bright, central core is always visible within ∼50 km of zero relative radius. The strands below the core are spiral in nature and are the sheared jets resulting from a collision in the F ring that we believe occurred in 2007. The more diffuse strands above the core are likely to be from older collisions. Each mosaic shows the channels that are a characteristic of the streamer-channel phenomenon produced by a recent passage of Prometheus (moving from left to right in this frame); Prometheus itself is in Figures 2(a) and (c). In each instance, the channel is ∼1° in azimuthal width (∼2450 km) and separated from the next channel by the characteristic wavelength of 3.°27. All mosaics show at least one "fan" indicating the presence (Murray et al. 2008) of an object embedded in the core perturbing nearby material (up to ∼200 km beyond the core). Furthermore, the base of each fan is located at the left-hand edge of a channel. The fans appear in material exterior to the ring's core implying a perturber with a semimajor axis near the inner edge of the core. Other processes including observational selection effects and proximity to Prometheus may account for the bias. Figures 2(b) and (c) show shadows associated with each fan, as well as bright objects in the inner strand, and, in Figure 2(c), all bright objects in the ring segment. The optical depth, τ, for the F ring core is ∼0.1 (Bosh et al. 2002). Theoretically, the maximum width of each fan channel

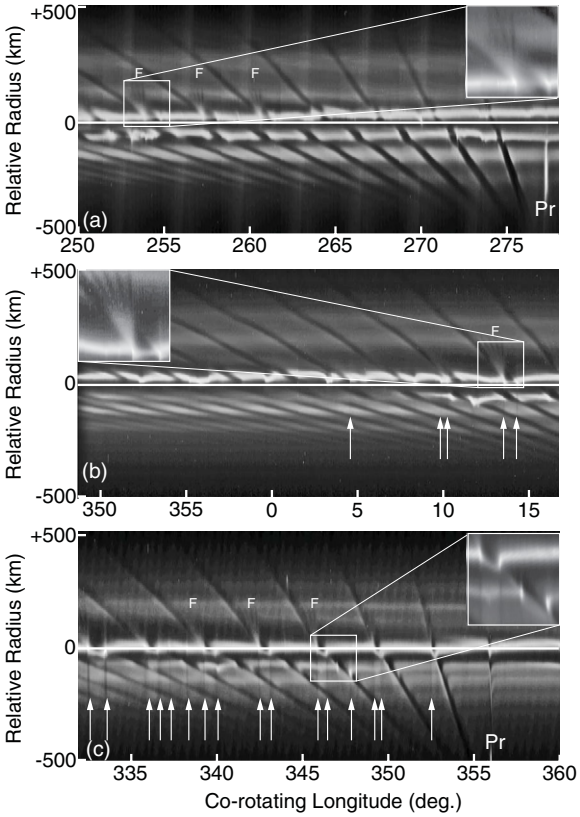

Figure 2. Mosaics of 28° sections of the F ring constructed from reprojected *Cassini* images, each showing evidence for embedded objects. "F" denotes a position above a "fan" (see the text) in the F ring's core indicating the presence of an embedded object. Images are shown in a corotating longitude system relative to the epoch of 2007 January 1 at 12 h UTC and have been enhanced to highlight features. The reprojected radius is shown with respect to the calculated orbital radius of the F rings core (Bosh et al. 2002). Images taken on (a) 2008 July 5 where three fans are visible, (b) 2008 December 8 where one fan is visible, and (c) 2009 April 16 where three fans are visible. Furthermore, faint shadows (indicated by arrows) are associated with several bright features in the ring: (b) and (c). The location of Prometheus is indicated by the letters Pr. In (b), Prometheus was located ∼3° to the right of the longitude range covered by the mosaic. The solar elevation angles in (a), (b), and (c) are −6.°2, −3.°8, and −1.°8, respectively. The estimated shadow lengths in (b) and (c) are 130–150 km and 200–240 km, respectively.

is known to be ∼10 times the Hill's radius of the embedded object (Murray et al. 2008; Williams 2009) implying a clump of mass (0.5–1.0) × 10^{16} kg produces the fan in Figure 2(b). FWHM measurements of the shadows in the raw images suggest a width of 73 ± 25 km. Measurements of shadow lengths in Figures 2(b) and (c) for the two solar elevation angles imply that they are caused by structures extending ∼5–10 km from the F ring plane. Together these observations are consistent with an azimuthally extended clump with mass comparable to that of an ∼10–20 km radius moonlet. The clear association of these objects with channel edges strongly suggests that Prometheus is responsible for their creation. Furthermore, the clumps persist until at least the next encounter with Prometheus (see Figure 1).

4. NUMERICAL MODELING

To understand this process, we carry out numerical integrations of test particles filling an ∼10° section of a 40 km-wide model F ring after it has undergone passage by Prometheus. The state of the ring segment at four separate times is shown in Figure 3. The times have been deliberately chosen to be at the

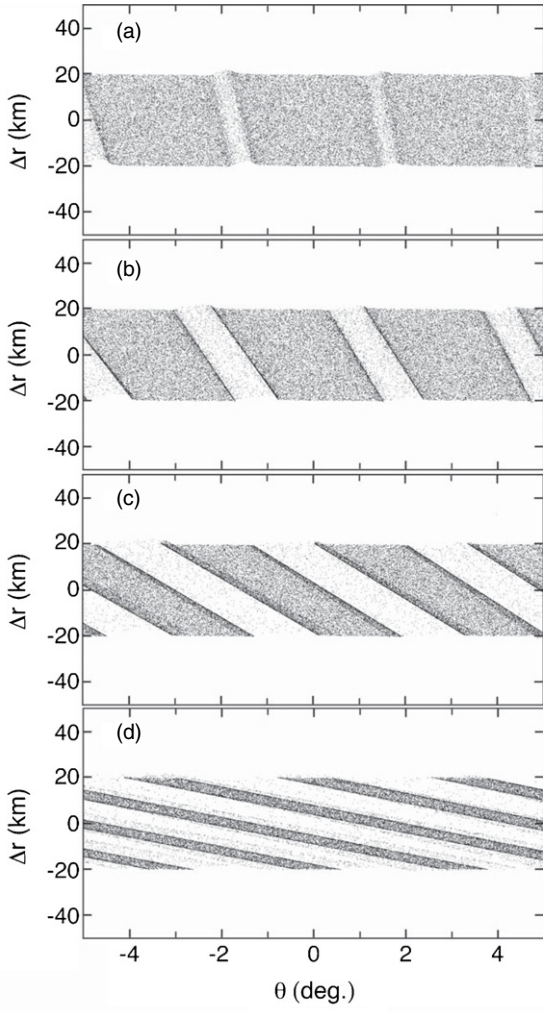

Figure 3. Evolution of a 10° segment of the F ring perturbed by Prometheus. The two-dimensional, collisionless numerical simulation of a 40 km wide ring was carried out with 50,000 test particles using orbits from Bosh et al. (2002) and Spitale et al. (2006). Δr, the radius with respect to the radial distance of the F ring, is shown as a function of θ, the corotating longitude. The units of time are given in Prometheus orbital periods (14.7 hr). The ring segment is shown at times (a) $t = 7.58$, (b) $t = 13.58$, (c) $t = 26.58$, and (d) $t = 70.58$ when Prometheus is closest to the core, roughly corresponding to that shown in Figure 2(a). Prometheus was at its periapse at $t = 0$.

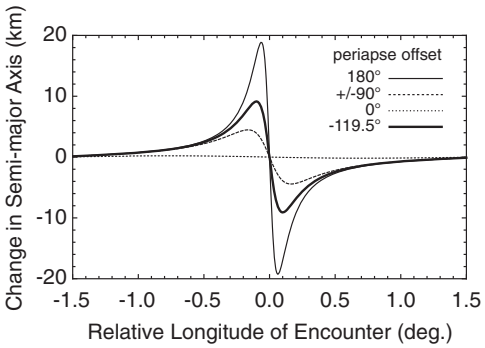

Figure 4. Changes in the semimajor axis, a, of F ring test particles perturbed by Prometheus. Numerical integrations of 3000 test particles encountering Prometheus over a range of 3.°27 (the wavelength of the periodic structure it produces) are used to calculate the changes in a in a two-dimensional model using mass and orbit data from Bosh et al. (2002) and Spitale et al. (2006). The integrations were performed for orbital alignment (minimum perturbation, $\varpi_r = 0$), orbital anti-alignment (maximum perturbation, $\varpi_r = 180°$, which occurred in late 2009), peripases at right angles ($\varpi_r = \pm 90°$) with respect to one another, and the configuration at the epoch of 2007 January 1, 12 hr when the difference in the periapses was $-119.°5$. In each case, the particle with the closest approach distance defines the zero relative longitude point. The corresponding changes in a as a function of the relative longitude of encounter are shown for each of the five configurations.

point within a cycle when the channels are most open. As previously demonstrated (Murray et al. 2005), the streamer-channel structure changes dramatically over one orbital period of the F ring particles (14.8 hr). Several effects are obvious in Figure 3: (1) there is a concentration of test particles at the edges of the channels at these points in the cycle, except for Figure 3(d) where particles are starting to leak into the channels; (2) the tilt of the channels continues to decline due to Keplerian shear; and (3) the channels get wider and consequently the ring sections between channels get narrower with time. All of these effects can be understood by undertaking a quantitative examination of the consequences of an encounter between F ring particles and Prometheus.

Figure 4 shows the changes in the semimajor axis, a, that result as Prometheus encounters a 3° section of the F ring in a numerical simulation for five different relative orientations of the two orbits. (Differential precession results in the periapses being anti-aligned every ∼19 years.) The method we used is similar to that of Showalter & Burns (1982). Our results show that the acquired changes in orbital elements depend on the separation at encounter and the relative orientation of the orbits. (The maximum changes in the semimajor axis, eccentricity, and longitude of periapse for different relative orientations were quoted in Murray et al. 2008.) The induced eccentricity change is comparable to that required to form fans. Furthermore, the sign of each change in the semimajor axis differs on either side of the zero relative longitude. In particular, if we consider the behavior of a within 0.°5 of the zero position close to the anti-alignment configuration, then a clear gradient of changes in a is imposed on either side with a maximum and minimum falling within ∼0.°1 of the center. Most importantly, $\Delta a > 0$ for negative relative longitude and $\Delta a < 0$ for positive relative longitude. (This is consistent with both directions of relative drift shown in Figure 1.) In our chosen frame, this results in material from the right edge moving to the right as material from the left edge moves to the left. This explains why the channels widen and the inter-channel regions narrow as the simulation progresses (Figures 3(a)–(c)); there is also evidence for this in Figure 2 where widening occurs as the separation from Prometheus (i.e., time since encounter) increases; see also Showalter & Burns (1982). Eventually the test particles from one channel edge meet the retreating edge from the next channel and start to fill the channel again (Figure 3(d)). While our simulations neglect the influence of the ring's self-gravity and collisions, this kinematic model suggests that the streamer-channel pattern created by Prometheus periodically triggers local increases in the surface density. This effect is particularly important at channel edges and may be sufficient to allow self-gravity to become effective and growth to occur in these regions. Nevertheless, future work explicitly including self-gravity and collisions would be useful in exploring how these processes influence the development and persistence of these condensations.

Cassini observations of both fans as well as bright regions capable of casting shadows at regions associated with perturbations by Prometheus all suggest circumstances in which gravitational condensations could occur. In Figure 5, we examine in detail how it is possible for the conditions for collapse to arise. The increase in the maximum number density following

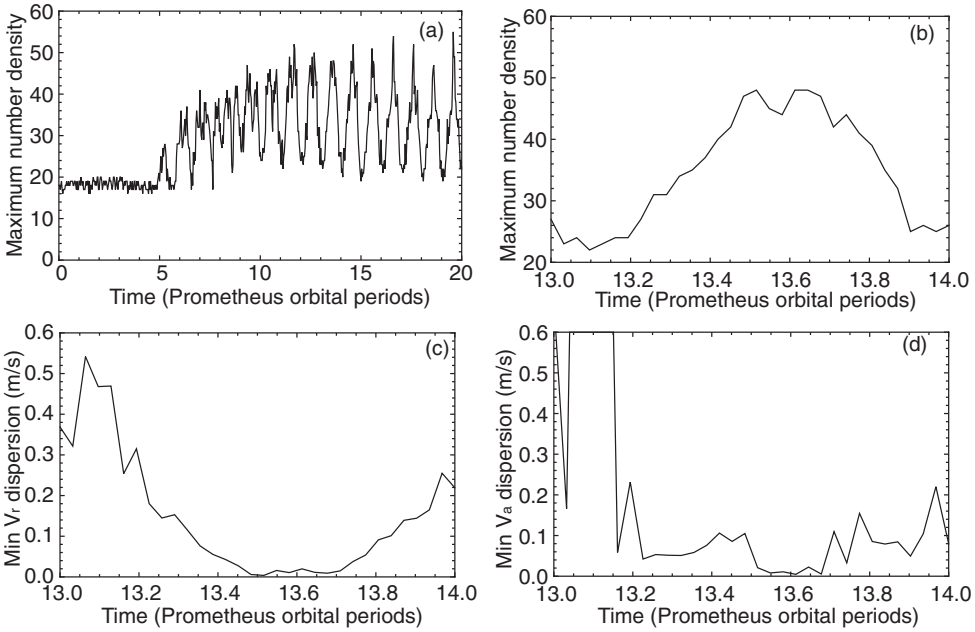

Figure 5. Time evolution of the ring segment showing changes in number density and velocity dispersion. The ring segment simulation shown in Figure 3 was divided into a grid of 200 × 100 boxes (in θ and r respectively), and at each time step the number density and dispersion in radial velocity of particles in each box was calculated. (a) The maximum density as a function of time; the large fluctuations are due to the radial oscillations in the rings width on the timescale of the orbital period. (b) The maximum number density over one orbital period (cf. Figure 3(b)). The minimum dispersion of the radial (c) and the azimuthal (d) velocity, V_r and V_a, respectively, of the test particles over the same orbital period as (b) for those cells with $\geqslant$20 particles. Note that the times when the velocity dispersion is at a minimum ($\leqslant$0.02 m s^{-1} at $t = 13.5$ and 13.7 compared with an escape velocity of $\sim$10 m s^{-1} for an $\sim$10 km icy satellite), the number density is close to a maximum.

the passage of Prometheus across the ring segment is clearly seen in Figure 5(a). Examination of the variation in maximum number density and the minimum values of the dispersion in the radial velocity over one cycle (Figures 5(b) and (c)) shows that near-zero dispersion in the radial velocity coincides with the times when the number density is at a maximum. It has been verified that this occurs for the same cells. The observed minimum values of the radial velocity dispersion ($\leqslant$0.02 m s^{-1}) are at least 2 orders of magnitude less than the escape velocity of an $\sim$10 km icy satellite implying that collisions would quickly result in a local condensation. Further, if Prometheus' perturbations create regions with bulk densities greater than the local Roche density ($= 3\rho(R/a)^3 \approx 0.15$ g cm^{-3} at the F ring, where ρ is the density of the planet, R is its radius) and low dispersion velocities, gravitational instability and collapse under self-gravity may occur. Note that this is equivalent to the conditions specified by the Toomre parameter (Toomre 1964; Karjalainen & Salo 2004; Lewis & Stewart 2009) frequently used in the context of stability in disks.[3]

[3] The Toomre stability parameter ($Q = v\Omega/\pi G\Sigma$, where Σ and v are the disk's surface density and dispersion velocity, respectively, Ω is the orbital angular frequency, and G is the gravitational constant) compares the strength of self-gravity relative to shear stresses and pressure support in an astrophysical disk. For $Q \lesssim 1$, gravitational instability may set in with collapse into coherent bound clumps possible. This instability criterion is functionally equivalent to requiring that the disk have a bulk density greater than the local Roche density (i.e., $\rho_d \gtrsim (3\rho_p)(R_p/a)^3$). This latter condition is commonly used in describing planetary ring systems. In a disk with scale height $H = v/\Omega$ the volume density near the mid-plane is approximately $\rho_d = \Sigma\Omega/v$. Using the primary density (ρ_p) and Kepler's third law yields $Q = (4/3)(\rho_p/\rho_d)(R_p/a)^3 \lesssim 1$, which is readily expressed as the Roche-like criterion $\rho_d \gtrsim (4/3)\rho_p(R_p/a)^3$. In this way, both the Toomre and Roche criteria compare the relative strengths of self-gravity and shear stresses.

5. AN EMERGING MODEL OF THE F RING

A picture of Prometheus' cumulative effect on the F ring now emerges. At the closest approach during each orbital period, the gravitational effect of the satellite significantly perturbs an $\sim$1° segment of the ring and the streamer-channel pattern is repeated every 3.°27. Each passage triggers the formation of objects at the channel edges and these now evolve with respect to the core of the F ring. The synodic period of this process is 67.6 days after which Prometheus returns to repeat the process, perturbing a different section of the ring, parts of which may already contain objects that have accreted material since their formation at previous encounters. Furthermore, we have detected bright objects and accompanying shadows around the ring implying that these objects can persist over several synodic periods. Particles suffer mutual collisions on a timescale of $t_{\rm col} \sim 1/\tau\Omega$, where Ω is the orbital frequency. So, optically thick regions, susceptible to gravitational instability, can dissipate relative velocities via inelastic collisions and become more tightly bound in a few orbital periods. The observational evidence suggests that, at least initially, these objects are formed by Prometheus and can be considered as coherent, enhanced density clumps which are still an integral part of the perturbed core, rather than fully formed moonlets. It is important to note that perturbations from Prometheus can also excite velocities between particles (note the variation over one cycle in Figure 5(c)). Depending on the phase, subsequent Prometheus encounters could either drive the disruption of such objects or enhance their growth; the balance of these processes ultimately gives rise to a characteristic distribution of different sizes observed in the present F ring (Murray et al. 2008).

The process by which Prometheus triggers local condensations in Saturn's F ring has direct applicability to the more general problem of accretion in systems such as a protoplanetary

disk being perturbed by a nascent protoplanet, where the embedded gas giant perturbs a marginally stable gas disk (Armitage & Hansen 1999). Gravitational instability provides a mechanism for the rapid formation of large bodies via the rapid collapse of an over-dense region of an astrophysical disk. Various modes of instability have been suggested to account for the formation of 10–100 km planetesimals (Goldreich & Ward 1973; Cuzzi et al. 2008; Johansen et al. 2007) and the formation of gas giant planets (Boss 2008). In this light, the clumps in the F ring may provide an observed celestial example of such an instability, at least in the case where gravitational growth is limited by the internal density and physical size of the particles. The sustained creation and destruction of these collapsing objects reveals the F ring as a natural laboratory for studying the processes that facilitate and frustrate such rapid growth.

This Letter is dedicated to the memory of K. Beurle. This work was funded by the UK Science and Technology Facilities Council and by NASA/JPL. We thank M. Showalter and the *Cassini* VIMS team for their invaluable help in obtaining observations. We also thank J. Burns and R. Nelson for useful discussions and suggestions.

Facilities: Cassini

REFERENCES

Armitage, P. J., & Hansen, B. M. 1999, Nature, 402, 633
Barbara, J. M., & Esposito, L. W. 2002, Icarus, 160, 161
Bosh, A., Olkin, C. B., French, R. G., & Nicholson, P. D. 2002, Icarus, 157, 57
Boss, A. P. 2008, Phys. Scr., T130, 014020
Canup, R. M., & Esposito, L. W. 1995, Icarus, 113, 331
Charnoz, S. 2009, Icarus, 201, 191
Charnoz, S., Porco, C. C., Deau, E., Brahic, A., Spitale, J. N., Bacques, G., & Baillie, K. 2005, Science, 310, 1300
Colwell, J. E., Esposito, L. W., & Sremcevic, M. 2006, Geophys. Res. Lett., 33, L07201
Cuzzi, J. N., & Burns, J. A. 1988, Icarus, 74, 284
Cuzzi, J. N., Hogan, R. C., & Shariff, K. 2008, ApJ, 687, 1432
Esposito, L. W., Meinke, B. K., Colwell, J. E., Nicholson, P. D., & Hedman, M. M. 2008, Icarus, 194, 278
Goldreich, P., & Ward, W. R. 1973, ApJ, 183, 1051
Hedman, M. M., Nicholson, P. D., Salo, H., Wallis, B. D., Buratti, B. J., Baines, K. H., Brown, R. H., & Clark, R. N. 2007, AJ, 133, 2624
Johansen, A., Oishi, J. S., Mac Low, M.-M., Klahr, H., Henning, T., & Youdin, A. 2007, Nature, 448, 1022
Karjalainen, R., & Salo, H. 2004, Icarus, 172, 328
Lewis, M. C., & Stewart, G. R. 2005, Icarus, 178, 124
Lewis, M. C., & Stewart, G. R. 2009, Icarus, 199, 387
Murray, C. D., & Dermott, S. F. 1999, Solar System Dynamics (Cambridge: Cambridge Univ. Press), 158
Murray, C. D., Beurle, K., Cooper, N. J., Evans, M. W., Williams, G. A., & Charnoz, S. 2008, Nature, 453, 739
Murray, C. D., Chavez, C., Beurle, K., Cooper, N., Evans, M. W., Burns, J. A., & Porco, C. C. 2005, Nature, 437, 1326
Porco, C. C., Weiss, J. W., Richardson, D. C., Dones, L., Quinn, T., & Throop, H. 2008, AJ, 136, 2172
Porco, C. C., et al. 2004, Space Sci. Rev., 115, 363
Porco, C. C., et al. 2005, Science, 307, 1226
Showalter, M. R., & Burns, J. A. 1982, Icarus, 52, 526
Showalter, M. R., Cuzzi, J. N., Marouf, E. A., & Esposito, L. W. 1986, Icarus, 66, 297
Spitale, J. N., Jacobson, R. A., Porco, C. C., & Owen, W. M. 2006, AJ, 132, 692
Toomre, A. 1964, ApJ, 139, 1217
Williams, G. A. 2009, PhD thesis, Queen Mary Univ. of London